

## Time-Resolved Multielectron Coincidence Spectroscopy of Double Auger-Meitner Decay Following Xe 4*d* Ionization


Pengju Zhang<sup>1,\*</sup>, Joel Trester<sup>1,†</sup>, Kiyoshi Ueda,<sup>1,2,3,†</sup> Meng Han,<sup>1,4</sup> Tadas Balčiūnas,<sup>1</sup> and Hans Jakob Wörner<sup>1,‡</sup>

<sup>1</sup>Laboratory for Physical Chemistry, ETH Zürich, Vladimir-Prelog-Weg 2, 8093 Zürich, Switzerland

<sup>2</sup>Department of Chemistry, Tohoku University, Sendai, 980-8578, Japan

<sup>3</sup>School Physical Science and Technology, ShanghaiTech University, Shanghai 201210, China

<sup>4</sup>J. R. Macdonald Laboratory, Department of Physics, Kansas State University, Manhattan, Kansas 66506, USA

 (Received 23 August 2023; revised 16 November 2023; accepted 24 January 2024; published 21 February 2024)

We introduce time-resolved multielectron coincidence spectroscopy and apply it to the double Auger-Meitner (AM) emission process following xenon 4*d* photoionization. The photoelectron and AM electron(s) are measured in coincidence by using a magnetic-bottle time-of-flight spectrometer, enabling an unambiguous assignment of the complete cascade pathways involving two AM electron emissions. In the presence of a near-infrared (NIR) laser pulse, the intermediate Xe<sup>2+\*</sup> state embedded in the Xe<sup>3+</sup> continuum is probed through single NIR photon absorption and the lifetime of this intermediate Xe<sup>2+\*</sup> state is directly obtained as (109 ± 22) fs.

DOI: [10.1103/PhysRevLett.132.083201](https://doi.org/10.1103/PhysRevLett.132.083201)

The creation of an inner-shell vacancy by high-energy photons initiates relaxation processes which can be either radiative or nonradiative. Electron correlation plays an essential role in the latter case, in which the unstable vacancy is filled by a valence electron and the released energy liberates another valence electron, the so-called Auger-Meitner (AM) electron [1]. It is well known that deep inner-shell vacancies prefer to decay by emission of two or more AM electrons, as demonstrated for various rare gases [2–10] and molecules [11–13]. In such cases, the unstable intermediate dication further decays into a triply charged ion. The interest in and significance of studying multiple AM emissions originate from the prominent role that electron correlation plays in the process.

As a consequence of the overlapping structures associated with different inner-shell states and the involvement of multiple AM decay pathways, accurately assigning individual decay pathways remains challenging. Therefore, the coincident detection of the photo- and AM electron(s) would be of great value to uniquely identify the inner-shell state, the intermediate dicationic state, as well as the final state, and thereby reveal the complete decay pathways. By utilizing a synchrotron light source, Penent *et al.* [8] exploited photo-AM-electrons coincidence spectroscopy to reveal that the cascade AM pathway dominates over the direct double AM emission upon Xe 4*d* photoionization. This study estimated a lower limit of 23 fs for the lifetime of the intermediate Xe<sup>2+\*</sup> state from the linewidth of its AM electron spectra.

Generally, such steady-state spectroscopic measurements can be limited by the instrumental resolution and influenced by the spectral asymmetries caused by postcollision interaction (PCI) [5,6,14–19]. Alternatively, studies of the cascade AM decay dynamics can be explicitly achieved

via time-resolved spectroscopic measurements [20–27], where the unstable inner-shell vacancy states are prepared through extreme-ultraviolet (XUV) photoionization and the electron emission is then dressed by an optical laser field, encoding information about the XUV pulse duration as well as the underlying relaxation dynamics. By measuring the time-dependent ion yields [23], the effective lifetime of the intermediate Xe<sup>2+</sup> doubly excited states ( $5p^{-4}nln'l'$ ) was found to be about 31 fs, which is in agreement with the result of energy-resolved measurements [8]. Nevertheless, the time-resolved ion-yield approach does not enable one to identify the intermediate levels thus delivering information that is averaged over all possible pathways. Therefore, the lifetimes of the individual intermediate states remained inaccessible.

In this Letter, we introduce time-resolved multielectron coincidence spectroscopy and demonstrate its potential through a direct time-resolved measurement of double AM emissions following Xe 4*d* photoionization. First, the photoelectron created by an XUV pulse (~91.5 eV) from a monochromatized high-harmonic source and two slow AM electrons were measured in coincidence and resolved in energy, providing the fingerprints of the various AM decay pathways. In the presence of a weak near-infrared (NIR) field, time-resolved multielectron coincidence spectroscopy was performed to further reveal the possible decay pathways of the intermediate Xe<sup>2+\*</sup> states, which enables us to draw a complete picture of the energetics of the double AM decay pathways, and especially to obtain the lifetime of the transiently populated Xe<sup>2+\*</sup> state. The energy diagrams associated with two AM emissions are presented in Fig. 1.

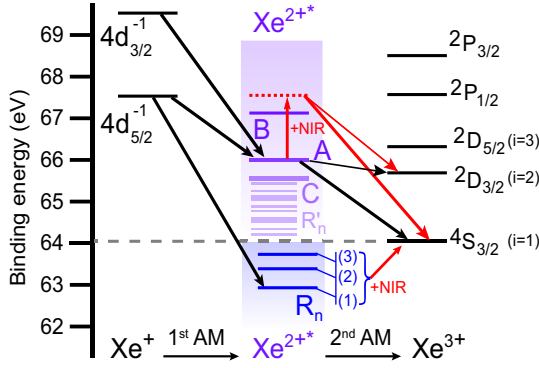


FIG. 1. Energy-level scheme for two AM emission pathways following Xe 4d photoionization. The  $\text{Xe}^{2+}$  states lying above and below the  $\text{Xe}^{3+}$  ( $4S_{3/2}$ ) ground state are denoted by the purple and blue areas, respectively (see details in the text).

The main features of the experimental setup have been described previously [28,29]. A fundamental NIR pulse (800 nm, 30 fs, 5 kHz) was divided by a beam splitter (70:30). The major portion ( $\sim 1.2$  mJ) was used for high-harmonic generation in a metallic tube (diameter  $\sim 4$  mm) filled with  $\sim 30$  mbar of neon gas, providing the XUV-pump pulse (H59, 91.5 eV). The minor portion, serving as the probe pulse, was independently focused on the gas jet in the second arm of the interferometer. The electrons were recorded by a magnetic-bottle photoelectron spectrometer equipped with a pair of microchannel plates (MCPs) in chevron configuration. In order to enhance the detection efficiency of the slow electrons ( $< 0.3$  eV), a bias potential (+0.3 V) was applied on the skimmer. The raw MCP waveforms were collected under extremely low count-rate conditions ( $\sim 0.11$ – $0.13$  counts/laser pulse) to minimize false coincidences. The individual signal waveforms were sorted into single, double, and multihit ( $\geq 3$ ) events. The triple-hit events ( $e_1, e_2, e_3$ ) were selected and further analyzed to illustrate the dynamics.

Figure 2 shows the coincidence spectra of the detected electron triples using an XUV photon energy of 91.5 eV. In the absence of the NIR field, the two-dimensional (2D) energy map is shown in Fig. 2(a) under the constraint of photoelectrons ionized from the  $4d_{3/2}$  ( $N_4$ ) shell. The color-coded histogram represents the number of the electron triples as a function of the faster AM electron energy ( $E_2$ ) on the horizontal axis and the slower AM electron energy ( $E_3$ ) on the vertical axis. Two characters are clearly observed in the 2D map. On the one hand, the diagonal stripe corresponding to a constant energy summation verifies the energy interval between the  $\text{Xe}^+$  hole state and the  $\text{Xe}^{3+}$  final states. The one-dimensional energy sum of the two AM electrons emitted in the presence of the XUV pulse only (“XUV only”) is shown in Fig. 2(c) as the solid black line, the peak positions are consistent with the energy levels of the  $\text{Xe}^{3+}$  final state [30]. On the other hand, all the diagonal stripes are dominated by

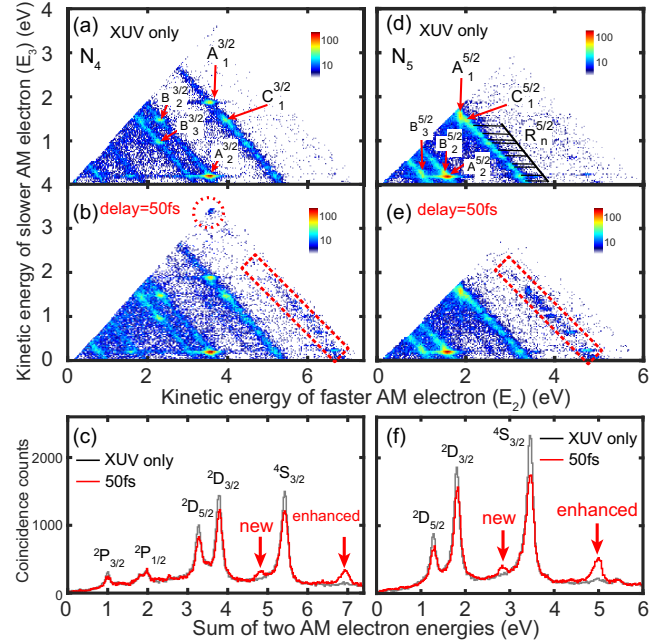


FIG. 2. Electron-electron-coincidence maps of double AM emission recorded following Xe 4d photoionization. The photoelectron ( $E_1$ ), and two AM electrons ( $E_2, E_3$ ) are measured in coincidence. The two-dimensional (2D) plots of the two AM electrons are presented according to the associated photoelectron. (a) and (b) show coincidence maps of two AM electrons from  $4d_{3/2}^{-1}$  with XUV only and a time delay of 50 fs, respectively. Positive delay represents that the NIR pulse follows the XUV pulse. (c) Summation of the two AM electron energies in panel (a) (black) and (b) (red), respectively. (d),(e),(f) Same as (a), (b), and (c) but from  $4d_{5/2}^{-1}$ . The number of detected electron triples in the 2D map is indicated by the color scale. The horizontal stripe at about 0.2 eV is caused by false coincidences.

discrete islands with rather weak continuous intensity distributions. This emphasizes the fact that the AM cascade decay dominates over the double AM process [31] and these islands suggest the necessity of considering intermediate  $\text{Xe}^{2+}$  states during the decay. For convenience, we label the individual islands by  $X_i^J$ , as suggested by Penet *et al.* [8], where  $i = 1$ – $3$  represents the energy level of the final  $\text{Xe}^{3+}$  state,  $J = 3/2$  or  $5/2$  denotes the total angular momentum quantum number ( $J$ ) of the  $\text{Xe}^+$   $4d^{-1}$  hole state, and  $A, B, C$  denote the intermediate states. The AM electron pairs associated with different intermediate  $\text{Xe}^{2+}$  states are listed in Table I. One needs to note that the AM electron energies are sorted such that  $E_2 \geq E_3$ .

Interestingly, in the presence of a weak NIR field, two distinct features emerge in the 2D energy map, i.e., a striplike region indicated by the red-dashed rectangle and an island denoted by the red-dashed circle, shown in Fig. 2(b) with a XUV-NIR time delay of 50 fs. The appearance of these coincidence events suggests that additional channels open up in the presence of the NIR field. Surprisingly, the energy sum of this NIR-induced

TABLE I. AM electron pairs of cascade decay from Xe  $4d$  holes (first column) with different final Xe $^{3+}$  states (first row). The intermediate states associated with two AM electrons  $X_i^J$  ( $E_2, E_3$ ) are shown in the middle. (Energies are given in eV).

Xe $^+$	Xe $^{3+}$					
	$^4S_{3/2}$ ( $i = 1$ ) (64.09)		$^2D_{3/2}$ ( $i = 2$ ) (65.73)		$^2D_{5/2}$ ( $i = 3$ ) (66.26)	
$N_4(3/2)$ (69.53)	$A_1$ (3.58, 1.88)	$C_1$ (3.95, 1.48)	$A_2$ (3.58, 0.22)	$B_2$ (2.31, 1.48)	$B_3$ (2.31, 0.98)	
$N_5(5/2)$ (67.55)	$A_1$ (1.88, 1.58)	$C_1$ (1.95, 1.48)	$A_2$ (1.58, 0.22)	$B_2$ (1.48, 0.31)	$B_3$ (0.98, 0.31)	

stripe is larger than the energy interval between the Xe $^+$  ( $N_4$ ) state and Xe $^{3+}$  ground state ( $^4S_{3/2}$ ), which will be explained below. The energy sum distribution is shown in Fig. 2(c) as the solid red line, which exhibits an enhanced peak around 6.92 eV corresponding to these two features marked in Fig. 2(b). Additionally, a new peak around 4.83 eV is showing up, which is not easily visible in the 2D map. Comparing with the  $N_4$  state, fewer pathways are observed during the decay of the  $4d_{5/2}^{-1}$  ( $N_5$ ) hole, which can be attributed to its smaller ionization potential. The multielectron spectra are shown in Figs. 2(d)–2(f), similarly, the NIR-induced coincidence events are also observed and show up both in the 2D map and in the 1D spectra. Importantly, the energy difference between the NIR-induced peak in Figs. 2(c) and 2(f) is consistent with the spin-orbit splitting between the  $N_4$  and  $N_5$  holes [32].

In order to assign the NIR-induced decay pathways, we performed a detailed analysis of the triple-coincidence events. In the case of the  $N_4$  state, i.e.,  $E_1 = E_{\text{XUV}} - IP(4d_{3/2}^{-1})$ , the faster and slower AM electron spectra are presented separately in Figs. 3(a) and 3(b), respectively. Ensuring full coverage of the NIR-induced events [see Fig. 2(b)], the energy-sum condition ( $\Sigma E_{\text{AM}}^{N_i}$ ) is chosen as  $E_2^{N_4} + E_3^{N_4} = [6.67.4]$  eV. The corresponding spectra are plotted for XUV only and XUV + NIR at a time delay of 50 fs. Comparing with the XUV-only spectra (in gray) in Fig. 3(a), it is clearly observed that the peak around 6.7 eV in the spectrum of the faster AM electron is enhanced and a new peak around 3.43 eV shows up in the same spectrum. In Fig. 3(b), a series of new peaks appears in the very low kinetic-energy region, which corresponds to the intensity increase in the region of  $E_2 > 6$  eV in Fig. 3(a). A new peak around 3.43 eV is also observed which originates from the absorption of one NIR photon by the A state (which creates the 1.88 eV AM electron by decaying to Xe $^{3+}$  ground state), thereby depleting the peak at 1.88 eV and creating an additional peak at 3.43 eV in Fig. 3(b). Specifically, under the energy-sum condition,  $E_2^{N_4} + E_3^{N_4} = [5.06.0]$  eV, the spectra of the faster AM electron are largely identical with and without NIR field [see Fig. 3(c)]. However a new peak appears around 1.78 eV in the spectrum of the slower AM electron [Fig. 3(d)], which originates from the absorption of one NIR photon by the A state, followed by a decay to the Xe $^{3+}$

$^2D_{3/2}$  cationic state. Because the two new peaks exclusively appear in the spectrum of the slower AM electron with respect to two different energy-sum conditions (see Table I), and the added energies perfectly match with one NIR photon energy ( $\sim 1.55$  eV); we believe that the NIR pulse probes the decay of the intermediate Xe $^{2+*}$  A state, which decays to either Xe $^{3+}$   $^4S_{3/2}$  or  $^2D_{3/2}$  state, leading to the increase of the second AM electron energy. This is further confirmed by the AM electron spectra from the  $N_5$  state, shown in Figs. 3(e)–3(h). Two new peaks are observed in the faster AM spectra and highlighted as insets of Figs. 3(e) and 3(g), and the energies of these peaks are identical to the ones from the  $N_4$  state.

Now, we discuss the origin of the series of new peaks in Figs. 3(b) and 3(f). As mentioned above, it is noticed that the energy sum associated with this series is larger than the

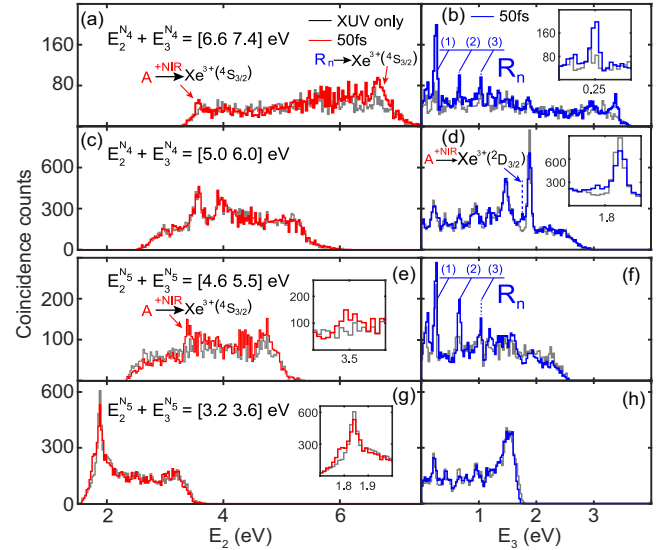


FIG. 3. One-dimensional double AM spectra under different energy-sum conditions. (a),(b) The spectra of the faster and slower AM electrons under the energy-sum condition:  $E_2^{N_4} + E_3^{N_4} = [6.67.4]$  eV. The black solid line denotes XUV photoionization only, the red and blue solid lines represent the results with the time delay at 50 fs. (c),(d) Same as (a),(b) under the condition:  $E_2^{N_4} + E_3^{N_4} = [5.06.0]$  eV. (e),(f) Same as (a),(b) but from  $4d_{5/2}^{-1}$  ( $N_5$ ) state under the condition  $E_2^{N_5} + E_3^{N_5} = [4.65.5]$  eV. (g),(h) Same as (e),(f) but with the condition  $E_2^{N_5} + E_3^{N_5} = [3.23.6]$  eV.



energy interval between its initial hole state and the threshold for the  $\text{Xe}^{3+}(^4S_{3/2})$  state, which suggests that the intermediate  $\text{Xe}^{2+*}$  states populated by the first AM emission might be energetically below the  $\text{Xe}^{3+}(^4S_{3/2})$  state, thus leading to the “first” AM electron with larger kinetic energy. Nevertheless, in the presence of the NIR field, a slow photoelectron is directly ionized from the intermediate  $\text{Xe}^{2+*}$  state to the  $\text{Xe}^{3+}$  ground state via single NIR absorption. Apparently, those  $\text{Xe}^{2+*}$  states manifest a Rydberg character, which should have a longer lifetime, compared to the typical AM lifetimes. These two aspects are actually further verified by the coincidence spectrum at larger time delays (see Sec. 1 in the Supplemental Material [33]).

The complete decay pathways with two sequential AM emissions are illustrated in Fig. 1. In the absence of the NIR field, the energy relaxation of  $\text{Xe}^+$   $4d$  holes leads to either intermediate  $\text{Xe}^{2+*}$  states lying above (purple) or below (blue) the threshold of  $\text{Xe}^{3+}$  state by AM emission. In the former case, these  $\text{Xe}^{2+*}$  states sequentially decay to different  $\text{Xe}^{3+}$  states with a second AM emission. However, the AM decay channel is energetically closed in the latter case. In the presence of the NIR field, the decay of the  $\text{Xe}^{2+*}$  states embedded in the  $\text{Xe}^{3+}$  continuum can be assisted or dressed by single NIR absorption, resulting in a laser-assisted Auger-Meitner decay into different  $\text{Xe}^{3+}$  states, whereas the  $\text{Xe}^{2+*}$  Rydberg states lying below  $\text{Xe}^{3+}(^4S_{3/2})$  state are directly ionized to the continuum.

Having verified the decay pathways, we performed a systematic time-resolved measurement to obtain the lifetimes of the intermediate  $\text{Xe}^{2+*}$  states. Taking into account the branching ratio for the formation of  $\text{Xe}^{3+}$  states [8], we choose the dominating AM decay pathway through the intermediate  $\text{Xe}^{2+*}$  A state to  $\text{Xe}^{3+} \ ^4S_{3/2}$ . Specifically, the absorption of an NIR photon from the A state leads to a new peak observed in the second AM spectrum around 3.43 eV [see Fig. 2(b)]. Under the fixed XUV-NIR time delay (50 fs), its yield is first measured with respect to different polarizations between the XUV-pump and NIR-probe pulses, which is shown in Fig. 4(a). The observed polarization-dependent yield implies the existence of orbital alignment in the A state produced by AM emission [34–36].

The time-dependent yield of the new peak originating from the A state is obtained and shown in Fig. 4(b). In principle, its time evolution includes two contributions, one is the exponential rise from the decay of  $\text{Xe}^+$   $4d$  hole states, the other one is the exponential decay to the  $\text{Xe}^{3+} \ ^4S_{3/2}$  state. Considering this sequential relaxation process [37,38], the decay profile can be fitted with the model function (see the details in the Supplemental Material [33]):

$$P(t) = [(p_1 e^{-t/\tau_1} + p_2(1 - e^{-t/\tau_1})e^{-t/\tau_2}) \times H(t)] \otimes G(t) \quad (1)$$

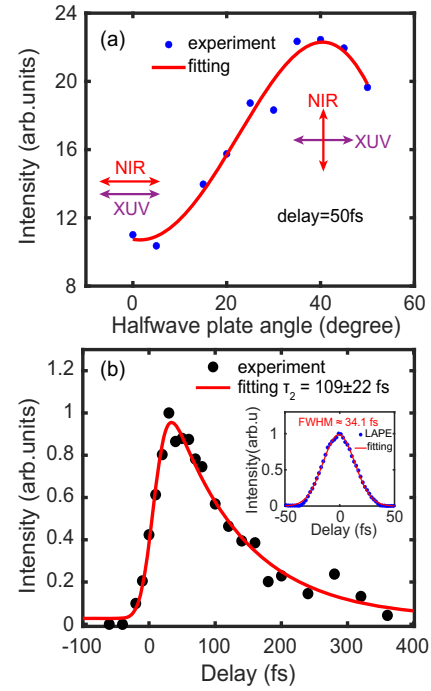


FIG. 4. (a) The NIR-induced peak intensity [see Fig. 3(b)] versus the polarization angle between the NIR and XUV pulses. The time delay is fixed at 50 fs. (b) The decay profile of the intermediate  $\text{Xe}^{2+*}$  A state. The inset shows the cross-correlation between the XUV (H59) and NIR pulses (see details in the text).

where  $p_1$  and  $p_2$  are the amplitude factors of the  $4d$  hole states and intermediate  $\text{Xe}^{2+*}$  A state,  $\tau_1$  and  $\tau_2$  are their lifetimes, respectively. The lifetime  $\tau_1$  is the same as the rise time of the  $\text{Xe}^{2+*}$  A state.  $H(t)$  is the Heaviside step function and the cross-correlation function between the XUV and NIR pulses is given by  $G(t)$ , which was determined by the laser-assisted photoelectric effect [39] (LAPE) of  $4d$  hole states ionized by a  $(1 + 1')$  XUV/NIR scheme [see the inset in Fig. 4(b)]. During the fitting procedure, the lifetime of the  $4d$  hole state was fixed to 6.1 fs [40], whereas  $p_1$ ,  $p_2$ , and  $\tau_2$  are fitting parameters. The fit of the data shown in Fig. 4(b) yields a lifetime of  $\tau_2 = 109 \pm 22$  fs. Comparing with the  $\sim 31$  fs lifetime of the  $\text{Xe}^{2+}$  doubly excited states ( $5p^{-4}nln'l'$ ) [23] lying above the threshold of the  $\text{Xe}^{3+} \ ^2P_{3/2}$  state, the lifetime of the A state is much longer, which is consistent with the availability of additional decay channels for the higher-lying excited states.

Before concluding, we discuss the configuration assignment of the A state. Because of the strong configuration interaction, the exact assignment of the A state has been a subject of debate for an extended period of time. A comparison between single- and multiconfiguration Dirac-Fock calculations [41] suggests that the intermediate  $\text{Xe}^{2+*}$  states slightly below the threshold of  $\text{Xe}^{3+}$  have a mixed character of  $5s^05p^6$ ,  $5s5p^45d$ , and  $5s^25p^25d^2$ .

While for the A state, Penent *et al.* [8] proposed that it could be the last member of the correlation AM satellites of  $5s^05p^6$ , leaving the exact configuration unassigned. Nevertheless, Uiberacker *et al.* [23] suggested that the A state is presumably  $5s5p^47p$ , and the Rydberg series below the threshold of the  $Xe^{3+}$  state could have either  $5s5p^46p$  or  $5s^25p^3nl$  configurations. Recently, taking into account the dynamic dipole polarization of electron shells, Petrov *et al.* [42] predicted that the configuration  $5s^25p^25d^2$  is the most likely one leading to the slow AM electron ( $< 5$  eV). Owing to the excellent energy agreement between this work and the calculation [42], we believe that the dominant configuration of the  $Xe^{2+*}$  A state should be  $5s^25p^25d^2(^1S_0)$ .

In summary, we have introduced time-resolved multi-electron coincidence spectroscopy and have applied it to study the cascaded double AM emission of Xe following  $4d$  photoionization. The multiple-coincidence spectra allow us to unambiguously disentangle the complete AM decay pathways. The lifetimes of the intermediate  $Xe^{2+*}$  states embedded in the  $Xe^{3+}$  continuum are directly obtained for the first time. This knowledge will be crucial for modeling electron correlation, in particular for three-electron interactions, leading to ultrafast AM decay. Our multielectron coincidence measurement in the time-domain develops a promising methodology to study the dynamics of multiple cascaded radiationless decay processes in atoms, molecules, and any system embedded in an environment, such as aqueous solutions. This technique will be particularly useful to temporally resolve the AM, intermolecular Coulombic decay (ICD) and electron-transfer-mediated decay (ETMD) processes that generally follow core-level or inner-shell ionization [43]. Our demonstration of time-resolved multielectron coincidence spectroscopy, coupled with emerging few-femtosecond to attosecond soft-x-ray sources, will provide time-domain access to these fundamental electron-correlation-driven decay processes that generally take place on timescales well below 10 fs [44].

We thank Professor Frédéric Merkt for the valuable discussions on the state assignment. We also thank Dr. Joss Wiese for the discussions on the kinetic model and Danylo Matselyukh for discussions on electron-electron correlation and coincidence as well as help with the beamline alignment. This work was supported by the European Research Council (Project No. 772797-ATTOLIQ), the Swiss National Science Foundation through the NCCR-MUST and Projects No. 200021\_172946 and No. 200020\_204928.

\* pengju.zhang@phys.chem.ethz.ch

† kiyoshi.ueda.a2@tohoku.ac.jp

‡ hwoerner@ethz.ch

[1] W. Mehlhorn, *J. Electron Spectrosc. Relat. Phenom.* **93**, 1 (1998).

- [2] T. A. Carlson and M. O. Krause, *Phys. Rev. Lett.* **14**, 390 (1965).
- [3] D. M. P. Holland, K. Codling, G. V. Marr, and J. B. West, *J. Phys. B* **12**, 2465 (1979).
- [4] N. Saito and I. H. Suzuki, *J. Phys. B* **25**, 1785 (1992).
- [5] P. Lablanquie, S. Sheinerman, F. Penent, R. I. Hall, M. Ahmad, Y. Hikosaka, and K. Ito, *Phys. Rev. Lett.* **87**, 053001 (2001).
- [6] P. Lablanquie, S. Sheinerman, F. Penent, R. I. Hall, M. Ahmad, T. Aoto, Y. Hikosaka, and K. Ito, *J. Phys. B* **35**, 3265 (2002).
- [7] S.-M. Huttula, S. Heinäsmäki, H. Aksela, E. Kukkk, M. Huttula, and S. Aksela, *Phys. Rev. A* **67**, 052703 (2003).
- [8] F. Penent, J. Palaudoux, P. Lablanquie, L. Andric, R. Feifel, and J. H. D. Eland, *Phys. Rev. Lett.* **95**, 083002 (2005).
- [9] Y. Hikosaka, P. Lablanquie, F. Penent, T. Kaneyasu, E. Shigemasa, J. H. D. Eland, T. Aoto, and K. Ito, *Phys. Rev. Lett.* **98**, 183002 (2007).
- [10] H. Fukuzawa, S.-K. Son, K. Motomura, S. Mondal, K. Nagaya, S. Wada, X.-J. Liu, R. Feifel, T. Tachibana, Y. Ito *et al.*, *Phys. Rev. Lett.* **110**, 173005 (2013).
- [11] A. Rudenko, L. Inhester, K. Hanasaki, X. Li, S. J. Robatjazi, B. Erk, R. Boll, K. Toyota, Y. Hao, O. Vendrell *et al.*, *Nature (London)* **546**, 129 (2017).
- [12] H. Fukuzawa, T. Takanashi, E. Kukkk, K. Motomura, S. ichi Wada, K. Nagaya, Y. Ito, T. Nishiyama, C. Nicolas, Y. Kumagai *et al.*, *Nat. Commun.* **10**, 2186 (2019).
- [13] P. J. Ho, D. Ray, C. S. Lehmann, A. E. A. Fouda, R. W. Dunford, E. P. Kanter, G. Doumy, L. Young, D. A. Walko, X. Zheng *et al.*, *J. Chem. Phys.* **158**, 134304 (2023).
- [14] H. Aksela, M. Kivilompolo, E. Nömmiste, and S. Aksela, *Phys. Rev. Lett.* **79**, 4970 (1997).
- [15] T. Carroll, J. Bozek, E. Kukkk, V. Myrseth, L. Sæthre, T. Thomas, and K. Wiesner, *J. Electron Spectrosc. Relat. Phenom.* **125**, 127 (2002).
- [16] R. Hentges, N. Müller, J. Viefhaus, U. Heinzmann, and U. Becker, *J. Phys. B* **37**, L267 (2004).
- [17] L. Partanen, M. Huttula, S. Heinäsmäki, H. Aksela, and S. Aksela, *J. Phys. B* **40**, 4605 (2007).
- [18] R. Guillemin, S. Sheinerman, C. Bomme, L. Journel, T. Marin, T. Marchenko, R. K. Kushawaha, N. Trcera, M. N. Piancastelli, and M. Simon, *Phys. Rev. Lett.* **109**, 013001 (2012).
- [19] L. Gerchikov, P. Lablanquie, J. Palaudoux, F. Penent, and S. Sheinerman, *Phys. Rev. A* **107**, 062822 (2023).
- [20] J. M. Schins, P. Breger, P. Agostini, R. C. Constantinescu, H. G. Muller, G. Grillon, A. Antonetti, and A. Mysyrowicz, *Phys. Rev. Lett.* **73**, 2180 (1994).
- [21] M. Drescher, M. Hentschel, R. Kienberger, M. Uiberacker, V. Yakovlev, A. Scrinzi, T. Westerwalbesloh, U. Kleineberg, U. Heinzmann, and F. Krausz, *Nature (London)* **419**, 803 (2002).
- [22] M. Drescher, M. Hentschel, R. Kienberger, M. Uiberacker, T. Westerwalbesloh, U. Kleineberg, U. Heinzmann, and F. Krausz, *J. Electron Spectrosc. Relat. Phenom.* **137–140**, 259 (2004).
- [23] M. Uiberacker, T. Uphues, M. Schultze, A. J. Verhoef, V. Yakovlev, M. F. Kling, J. Rauschenberger, N. M. Kabachnik, H. Schröder, M. Lezius *et al.*, *Nature (London)* **446**, 627 (2007).

- [24] T. Uphues, M. Schultze, M. F. Kling, M. Uiberacker, S. Hendel, U. Heinzmann, N. M. Kabachnik, and M. Drescher, *New J. Phys.* **10**, 025009 (2008).
- [25] M. Krikunova, T. Maltezopoulos, A. Azima, M. Schlie, U. Frühling, H. Redlin, R. Kalms, S. Cunovic, N. M. Kabachnik, M. Wieland *et al.*, *New J. Phys.* **11**, 123019 (2009).
- [26] A. J. Verhoef, A. V. Mitrofanov, X. T. Nguyen, M. Krikunova, S. Fritzsche, N. M. Kabachnik, M. Drescher, and A. Baltuška, *New J. Phys.* **13**, 113003 (2011).
- [27] S. Zherebtsov, A. Wirth, T. Uphues, I. Znakovskaya, O. Herrwerth, J. Gagnon, M. Korbman, V. S. Yakovlev, M. J. J. Vrakking, M. Drescher *et al.*, *J. Phys. B* **44**, 105601 (2011).
- [28] A. von Conta, M. Huppert, and H. J. Wörner, *Rev. Sci. Instrum.* **87**, 073102 (2016).
- [29] P. Zhang, C. Perry, T. T. Luu, D. Matselyukh, and H. J. Wörner, *Phys. Rev. Lett.* **128**, 133001 (2022).
- [30] A. Tauheed, Y. N. Joshi, and E. H. Pinnington, *Phys. Scr.* **47**, 555 (1993).
- [31] J. Viefhaus, M. Braune, S. Korica, A. Reinköster, D. Rolles, and U. Becker, *J. Phys. B* **38**, 3885 (2005).
- [32] G. C. King, M. Tronc, F. H. Read, and R. C. Bradford, *J. Phys. B* **10**, 2479 (1977).
- [33] See Supplemental Material at <http://link.aps.org/supplemental/10.1103/PhysRevLett.132.083201> for a discussion of the long-lived Rydberg series and the kinetic model of the A-state population.
- [34] N. M. Kabachnik, J. Tulkki, H. Aksela, and S. Ricz, *Phys. Rev. A* **49**, 4653 (1994).
- [35] M. Meyer, A. Marquette, A. N. Grum-Grzhimailo, U. Kleiman, and B. Lohmann, *Phys. Rev. A* **64**, 022703 (2001).
- [36] L. Budewig, S.-K. Son, and R. Santra, *Phys. Rev. A* **105**, 033111 (2022).
- [37] S. Karashima, Y.-I. Suzuki, and T. Suzuki, *J. Phys. Chem. Lett.* **12**, 3755 (2021).
- [38] C. Wang, M. D. J. Waters, P. Zhang, J. Suchan, V. Svoboda, T. T. Luu, C. Perry, Z. Yin, P. Slavíček, and H. J. Wörner, *Nat. Chem.* **14**, 1126 (2022).
- [39] V. Véniard, R. Taïeb, and A. Maquet, *Phys. Rev. Lett.* **74**, 4161 (1995).
- [40] M. Jurvansuu, A. Kivimäki, and S. Aksela, *Phys. Rev. A* **64**, 012502 (2001).
- [41] H. Aksela, S. Aksela, and H. Pulkkinen, *Phys. Rev. A* **30**, 865 (1984).
- [42] I. D. Petrov, B. M. Lagutin, V. L. Sukhorukov, A. Ehresmann, and H. Schmoranzner, *J. Phys. B* **47**, 055001 (2014).
- [43] I. B. Müller and L. S. Cederbaum, *J. Chem. Phys.* **122** (2005).
- [44] K. Gokhberg, A. I. Kuleff, and L. S. Cederbaum, in *Molecular Spectroscopy and Quantum Dynamics* (Elsevier, Amsterdam, 2021), pp. 163–197.